nature physics

LETTERS

PUBLISHED ONLINE: 1 AUGUST 2016 | DOI: 10.1038/NPHYS3835

Many-body interferometry of a Rydberg-dressed spin lattice

Johannes Zeiher[1], Rick van Bijnen[2], Peter Schauß[1], Sebastian Hild[1], Jae-yoon Choi[1], Thomas Pohl[2], Immanuel Bloch[1,3] and Christian Gross[1]*

Ultracold atoms in optical lattices are ideal to study fundamentally new quantum many-body systems[1,2] including frustrated or topological magnetic phases[3,4] and supersolids[5,6]. However, the necessary control of strong long-range interactions between distant ground state atoms has remained a long-standing goal. Optical dressing of ground state atoms via off-resonant laser coupling to Rydberg states is one way to tailor such interactions[5–8]. Here we report the realization of coherent Rydberg dressing to implement a two-dimensional synthetic spin lattice. Our single-atom-resolved interferometric measurements of the many-body dynamics enable the microscopic probing of the interactions and reveal their highly tunable range and anisotropy. Our work marks the first step towards the use of laser-controlled Rydberg interactions for the study of exotic quantum magnets[3,4,9] in optical lattices.

Neutral ultracold atoms in optical lattices are among the most promising platforms for the implementation of analog quantum simulators of condensed matter systems. However, the simulation of magnetic Hamiltonians, often emerging as an effective model in more complex many-body systems, is difficult with contact interactions due to the low energy scale of the associated superexchange process[10]. Long-range interactions offer an alternative way to directly achieve strong effective spin–spin interactions. Such interactions emerge between magnetic atoms and between ultracold polar molecules[11], trapped ions[12] or ground state atoms resonantly[13] or off-resonantly coupled ('dressed') to Rydberg states[5–8]. Rydberg dressing is especially appealing due to the simplicity of realizing atomic lattice systems with unity filling, combined with the great tunability of the interaction strength and shape, which might be exploited to explore exotic models of quantum magnetism[3,4]. While effects of long-range spin interactions have been observed in many-body systems of polar molecules[14], ions[15–17] and resonantly excited Rydberg atoms[18,19], none of these approaches combines the advantages of Rydberg dressing, which permits the realization of strong spin interactions in lattices with near-unity filling. So far, Rydberg dressing in a many-body system remains an experimental challenge, for which up to now only dissipative effects have been measured[20–24]. For two atoms, first promising experimental results have been reported recently for near-resonant strong dressing[25], where, however, the assumption of a weak Rydberg-state admixture required for the realization of various many-body models[5,6,9,26,27] does not hold[28].

Here we demonstrate Rydberg dressing in a two-dimensional (2D) near-unity-filled atomic lattice with tailored extended range interactions between approximately 200 effective spins. In contrast to our previous experiments[18,29] on resonantly coupled Rydberg gases, all atoms participate here in the spin dynamics. We exploit the temporal control over such interactions to perform interferometric measurements on the many-body system that directly reveal the induced correlations via single-site-sensitive local detection[30]. Our experiments illustrate the versatility of Rydberg dressing by tuning the range and isotropy[31,32] of the interaction potential induced by optical coupling to high-lying P-states. First-principles potential calculations together with an exact solution of the many-body dynamics accurately reproduce these measurements. From this we conclude that stimulated Rydberg–Rydberg state transitions, recently observed as anomalous broadening[24], act collectively in a many-body system, implying that rare one-body decay events can globally affect the entire spin lattice.

Dressed atomic states emerge as new eigenstates of an atom driven by a laser field with a Rabi frequency Ω and frequency detuning Δ. Considering two levels $|g\rangle$ and $|e\rangle$ in the weak dressing regime, $\Omega \ll \Delta$, the dressed ground state $|\tilde{g}\rangle \approx |g\rangle + \beta|e\rangle$ contains a small admixture $\beta = \Omega/(2\Delta)$ of the state $|e\rangle$. As a result, it acquires a finite lifetime τ_r/β^2, which, however, greatly exceeds the lifetime τ_r of the bare excited state. Choosing $|e\rangle$ to be a Rydberg state, the laser coupling also induces effective interactions between two dressed atoms in state $|\tilde{g}\rangle$ (Fig. 1a). At large interatomic distances $\boldsymbol{R}$ this interaction, $U(\boldsymbol{R}) \approx \beta^4 V(\boldsymbol{R})$, corresponds to the Rydberg–Rydberg atom interaction potential $V(\boldsymbol{R})$ reduced by the probability β^4 to excite both atoms at once. At short distances, however, the strong interaction between Rydberg atoms blocks this simultaneous excitation within a critical distance, R_c, determined by $V(R_c) = 2\hbar\Delta$. As a result, the induced interaction acquires a soft-core shape and saturates to a value of $U_0 = \hbar\Omega^4/(8|\Delta|^3)$ (Fig. 1c)[5,6,8]. Involving other atomic ground states in the dynamics, one naturally obtains various kinds of lattice models of interacting spins that have been proposed for metrology applications[8,33] or the exploration of exotic quantum magnetism[3,4]. In the simplest case, a single additional ground state that is not coupled to the Rydberg state (Fig. 1a,b) results in a system described by a 2D Ising Hamiltonian

$$\hat{H} = \hbar \sum_{i}^{N} \left(\delta + \Delta_i^{(\mathrm{coll})}\right) \hat{S}_i^z + \sum_{(i \neq j)}^{N} \frac{U_{i,j}}{2} \hat{S}_i^z \hat{S}_j^z \qquad (1)$$

Here, $\hat{S}^z$ is a spin-1/2 operator with eigenstates $|\uparrow\rangle$ and $|\downarrow\rangle$, corresponding to the Rydberg-dressed and uncoupled atomic ground state, respectively. The longitudinal field δ arises from the single-atom light shift, $\delta \approx \Omega^2/(4\Delta)$ and $U_{i,j} = U_0/(1 + (R/R_c)^6)$ denotes the dressing-induced interaction between spins located on lattice sites $\boldsymbol{i}$ and $\boldsymbol{j}$ at a distance $R/a_{\mathrm{lat}} = |\boldsymbol{i} - \boldsymbol{j}|$, where a_{lat} denotes the lattice constant. The collective contribution $\Delta_i^{(\mathrm{coll})} = \sum_{j \neq i}^{N} (U_{i,j}/2)$

[1]Max-Planck-Institut für Quantenoptik, Hans-Kopfermann-Straße 1, 85748 Garching, Germany. [2]Max-Planck-Institut für Physik komplexer Systeme, Nöthnitzer Straße 38, 01187 Dresden, Germany. [3]Ludwig-Maximilians-Universität, Fakultät für Physik, Schellingstraße 4, 80799 München, Germany. *e-mail: christian.gross@mpq.mpg.de

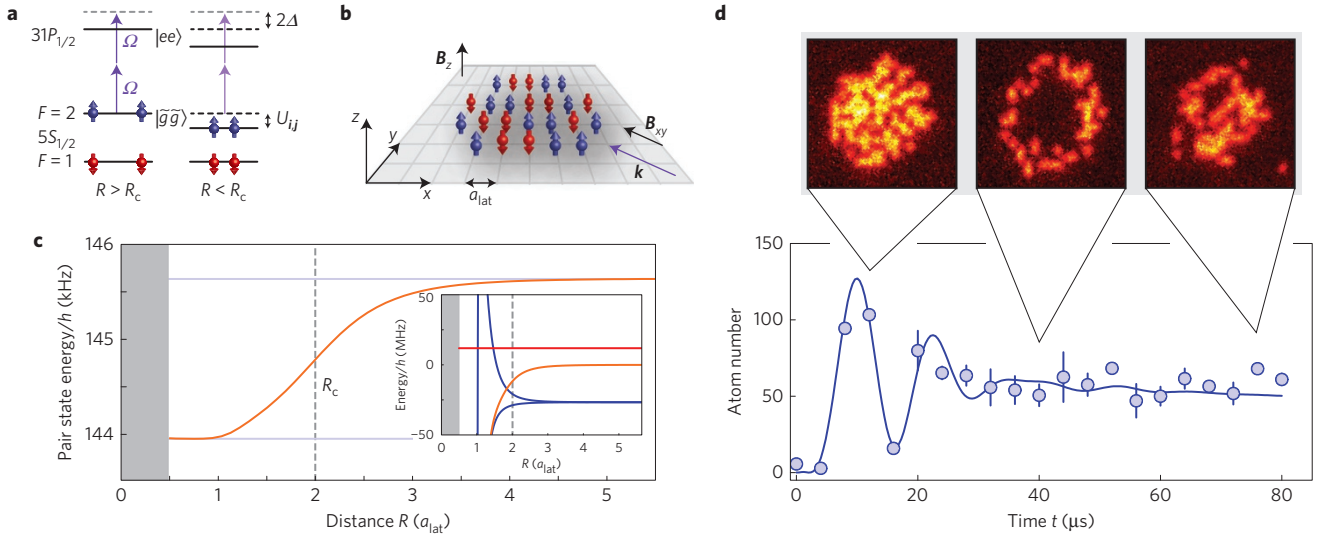

Figure 1 | Schematic of the experiment. a, The $5S_{1/2}|F=2, m_F=-2\rangle$ state (spin up $|\uparrow\rangle$, blue arrow) is coupled to a Rydberg state $|e\rangle$ in the manifold of $31P_{1/2}$ with Rabi frequency Ω (purple arrow) and detuning Δ (upper black arrow), leading to the dressed state $|\tilde{g}\rangle$. For separations $R < R_c$, the bare Rydberg interactions detune the state $|ee\rangle$ with two atoms in $|e\rangle$ (shifted black solid line), which is two-photon-coupled via the singly excited intermediate state. This induces interactions $U_{i,j}$ between ground state atoms in $|\uparrow\rangle$ whereas the spin down state $|\downarrow\rangle$ ($|1,-1\rangle$, red arrow) remains unaffected. **b**, The excitation laser propagates along $\boldsymbol{k}$ in the plane of the 2D spin lattice (lattice constant a_{lat}) at an angle of 45° with respect to the x and y axes. The magnetic field $\boldsymbol{B}_z$ ($\boldsymbol{B}_{xy}$) was aligned with the z-axis ($\boldsymbol{k}$). **c**, Calculated soft-core potential for $31P_{1/2}$ for $\Omega_s/2\pi = 1.33$ MHz and $\Delta/2\pi = 6$ MHz (orange solid line). The AC-Stark shift of the pair state and the soft-core saturation value U_0 are shown as the upper and lower horizontal light blue line respectively. The inset shows the bare Rydberg interaction curves (blue solid lines), including the optically coupled potential (orange solid line) underlying the soft-core interaction. R_c (vertical dashed line) marks the distance where the interaction shift equals 2Δ (red solid line). The grey shading indicates the region where crossings of other Rydberg states are expected, leading to slight modifications of the soft-core at distances well below a_{lat} (Supplementary Fig. 4). **d**, Ramsey oscillation fringe with $|\uparrow\rangle$ coupled to $31P_{3/2}$, $m_J = -3/2$ with $\Omega_s/2\pi = 1.9(1)$ MHz and $\Delta/2\pi = -8$ MHz (blue points). Three representative single shots of the atom distributions at the times indicated by the grey triangles are shown above. In the central shot, the bulk part of the sample had acquired a relative phase shift of π with respect to particles situated at the edge due to the collective longitudinal field $\Delta_i^{(coll)}$. The theory prediction (solid blue line) reproduces the interaction-induced dephasing of the oscillation. The error bars denote the standard error of the mean (s.e.m.).

results from the transformation from the original atomic-state representation to effective spin operators[18,34]. The interaction-induced energy shift resulting from this additional longitudinal field is measurable as a frequency shift in an interferometric Ramsey sequence (Supplementary Figs 1 and 2). Furthermore, due to the extended range of the interactions, this collective field depends on the spins nearby; hence, spins near the edge of a finite system evolve differently compared to spins in the centre. We directly observe this as an inhomogeneous spin distribution significantly contributing to dephasing of the Ramsey fringe (Fig. 1d).

The optically switchable spin interactions $U_{i,j} \propto \Omega(t)^4$ enable such interferometric measurements of the many-body system by sequential application of the interaction Hamiltonian equation (1) and a transverse magnetic field induced by microwave coupling of the two ground states[33,35].

Our experiments started with a 2D degenerate gas of rubidium-87 in the $|F, m_F\rangle = |1,-1\rangle$ hyperfine state, confined in a single antinode of a vertical (z-axis) optical lattice. In this single x–y plane, we then switched on a square optical lattice with $a_{lat} = 532$ nm spacing and prepared about 190 atoms in a unity-filling Mott insulator with a defect fraction of about 3%. The chosen atom number ensured a negligibly small number of doubly occupied sites. Transitions from the state $|1,-1\rangle$ ('spin down', $|\downarrow\rangle$) to $|2,-2\rangle$ ('spin up', $|\uparrow\rangle$) were driven globally via microwave pulses. To introduce long-range interactions, the state $|\uparrow\rangle$ was laser-coupled to the $31P_J$ state ($J = 1/2$ or $J = 3/2$), which has a lifetime of approximately $\tau_r = 27$ μs (see ref. 36). The excitation beam at a wavelength of 297 nm propagated in the plane of the atoms along the diagonal of the cubic lattice (Fig. 1b). A static magnetic field was used to set the quantization axis either along the z-direction or aligned with the laser beam wavevector $\boldsymbol{k}$, which allowed selective coupling to different Rydberg states, depending on the polarization of the excitation beam (Supplementary Fig. 3 and Supplementary Information). The positions of all the atoms were then detected with single-lattice-site resolution and single-atom sensitivity[37]. By optically removing atoms in state $|\uparrow\rangle$ before imaging, we could also perform spin-resolved detection and, in particular, measurements of spin–spin correlations.

In a first experiment, we aim to reveal the characteristic spin correlations in the many-body system that emerge over time as a result of the long-ranged spin interactions. To this end, we employ an interferometric spin-echo sequence (Supplementary Fig. 1), which is sensitive to interaction-induced phase shifts, whereas the influence of single-particle effects including the collective longitudinal field (Fig. 1d) is suppressed. Starting with all atoms in state $|\downarrow\rangle$ we first applied a $\pi/2$ microwave pulse on the $|\downarrow\rangle - |\uparrow\rangle$ transition to generate an equal superposition of the two spin states. This was followed by two identical Rydberg-dressing pulses of duration $t/2$ each, separated by a π microwave pulse. After closing the interferometer with another $\pi/2$ pulse, in the absence of interactions the system returns to its initial state with all the population in $|\downarrow\rangle$, such that any deviations from this are expected to provide a precise probe of the interaction-induced dynamics described by the Hamiltonian equation (1). Optical dressing to the $31P_{1/2}$ Rydberg state was performed with a detuning $\Delta/2\pi = 6$ MHz and a Rabi frequency of $\Omega_s/2\pi = 1.33(7)$ MHz, determined independently by Ramsey interferometry (Supplementary Fig. 2 and Supplementary Information). These laser parameters ensure the system is in the weak dressing regime with a small Rydberg-state admixture of $\beta = 0.11(1)$, corresponding to a population probability of $\beta^2 = 0.012(2)$. The resulting long-range spin interactions with $U_0/2\pi \approx 1.8$ kHz induce correlated phase rotations during the two

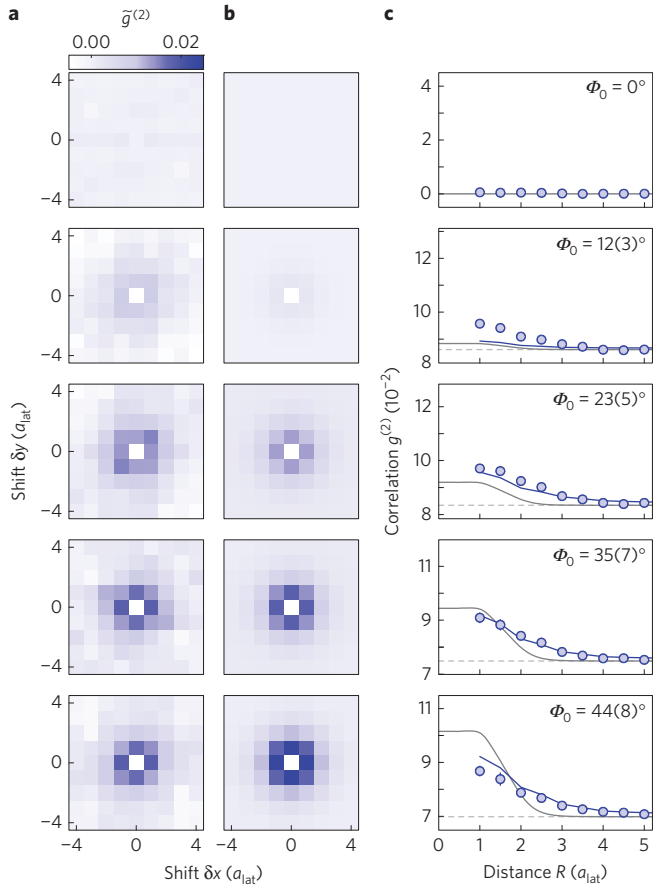

Figure 2 | Interferometric measurement of spin–spin correlation. **a**, Measured 2D spin correlation functions $\tilde{g}^{(2)}(\boldsymbol{R}) = g^{(2)}(\boldsymbol{R}) - g^{(2)}_{\infty}$ for increasing interaction phase Φ_0 (top to bottom) evaluated in a region of interest of 9×9 lattice sites. The constant spatial offset $g^{(2)}_{\infty}$ was obtained by azimuthally averaging $g^{(2)}(\boldsymbol{R})$ for $4.5 \leq |\boldsymbol{R}|/a_{\mathrm{lat}} \leq 7.5$ and subtracted for each data set. The two axes are the shifts $\boldsymbol{R} = (\delta x, \delta y)$. **b**, Theory prediction for $\tilde{g}^{(2)}(\boldsymbol{R})$ including dissipation with $g^{(2)}_{\infty}$ adjusted to the experimentally determined value. **c**, Azimuthal averages of the 2D correlations in **a** (blue points), and **b** (blue solid line) versus distance $R = |\boldsymbol{R}|$. The perturbative estimate (solid dark grey line) shifted by $g^{(2)}_{\infty}$ (dashed light grey line) differs significantly from the non-perturbative prediction for the spin correlation (see main text). The shown correlations were extracted from 250 to 300 experimental shots. All error bars denote the s.e.m.

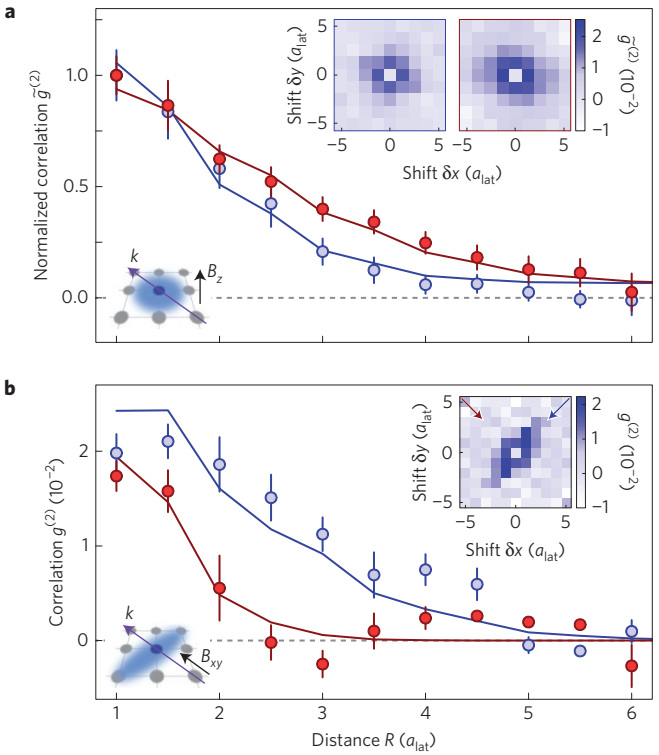

Figure 3 | Tunability of the long-range interaction. **a**, Comparison of the azimuthally averaged normalized spin correlation $\tilde{g}^{(2)}$ for $31P_{1/2}$ (blue points) and $31P_{3/2}$ (red points) together with theory predictions (blue and red solid lines, $\Delta/2\pi = 6$ MHz, $\Omega_s/2\pi = 1.33(7)$ MHz, $\Phi_0 = 35(7)°$ ($\Delta/2\pi = -6$ MHz, $\Omega_s/2\pi = 1.16(6)$ MHz, $\Phi_0 = 22(5)°$) for $J = 1/2$ (3/2)). The inset shows the 2D correlations for the two cases $J = 1/2$ (left) and $J = 3/2$ (right). The inset in the lower left corner illustrates the excitation geometry with the magnetic field along z (black arrow) and the excitation beam (purple arrow) in the atomic plane (grey discs), which leads to isotropic interaction (light blue area). The shown correlation was extracted from 180 experimental shots. **b**, One-dimensional averages of an anisotropic spin correlation along two orthogonal directions (red and blue points), obtained by averaging two neighbouring sites, together with the prediction of the coherent theory without dissipation (red and blue solid lines, $\Omega_s/2\pi = 2.45(12)$ MHz, $\Delta/2\pi = -12$ MHz and $\Phi_0 = 42(9)°$). The inset shows the 2D correlation, with the two averaging directions indicated by red and blue arrows. Post-selection was applied before calculating the correlation on a set of 20 images (Supplementary Fig. 7). The inset in the lower left corner indicates the geometry as in **a**. All error bars denote the s.e.m.

dressing stages peaking at $\Phi_0 = \int_0^t U_0(\tilde{t})\,\mathrm{d}\tilde{t}$, and ultimately lead to measurable spin correlations at the end of the interferometric echo sequence. The time dependence of U_0 arises from the finite rise time of Ω. Our spin-resolved detection scheme provides direct access to longitudinal correlations $g^{(2)}_{i,j} = \langle \hat{\sigma}^{(i)}_{\downarrow\downarrow} \hat{\sigma}^{(j)}_{\downarrow\downarrow} \rangle - \langle \hat{\sigma}^{(i)}_{\downarrow\downarrow} \rangle \langle \hat{\sigma}^{(j)}_{\downarrow\downarrow} \rangle$, where $\hat{\sigma}^{(i)}_{\downarrow\downarrow}$ measures the $|\downarrow\rangle$-population at site $\boldsymbol{i}$. Measurements versus time or, equivalently, versus the interaction phase Φ_0 permit the dynamical growth of the spin–spin correlations to be traced in the regime of small interaction phase, whereas for large Φ_0 the correlation signal is expected to decrease. Figure 2a shows the measured spin correlation function $g^{(2)}(\boldsymbol{R}) = \sum_{i \neq j} \delta_{ij,\boldsymbol{R}}\, g^{(2)}_{i,j} / \sum_{i \neq j} \delta_{ij,\boldsymbol{R}}$, which is obtained from a translational average constrained to a given distance $\boldsymbol{R}$ by the Kronecker symbol $\delta_{ij,\boldsymbol{R}}$. The observed correlation functions resemble the soft-core-shaped interaction potential shown in Fig. 1c. This behaviour is readily understood in the short-time limit for $N_{\mathrm{eff}}\Phi_0^2 \ll 1$, where N_{eff} denotes the number of spins within the range R_c of the interaction potential. In this short-time limit, one obtains a direct proportionality $g^{(2)}(R) = \Phi_0^2/(4(1 + (R/R_c)^6)^2)$ between the induced correlations and the square of the soft-core potential. However, for all non-zero interaction times probed in the experiment, the correlations deviate from this simple expression due to the presence of surrounding spins (Fig. 2c), as reproduced by the analytic theory (see Supplementary Information). This directly highlights the importance of many-body effects in our long-range interacting system despite the seemingly small interaction phases.

Next to the optical switchability, Rydberg dressing also enables designing the extent and anisotropy of the interactions between the spins. In the following, we demonstrate this control capability by selecting different coupled Rydberg states. As shown in Fig. 3a, changing the Rydberg state from $31P_{1/2}$ to $31P_{3/2}$ leads to notable modifications of the measured correlation function and, hence, the underlying spin interactions. In contrast to $31P_{1/2}$, the $31P_{3/2}$ state features repulsive interactions with a tenfold larger magnitude (Supplementary Fig. 4), which implies a 50% larger interaction radius $R_c/a_{\mathrm{lat}} \approx 3$ that is reflected in the enhanced correlation range shown in Fig. 3a. In both cases, the angular symmetry of the induced

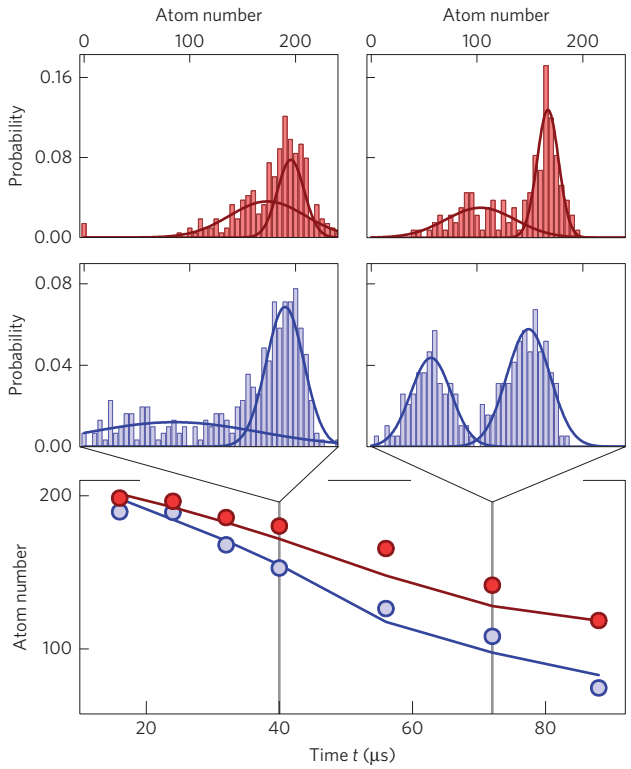

Figure 4 | Collective dissipation. Extracted mean atom number after a spin-echo sequence versus dressing time t with and without spin-resolved detection (blue and red points respectively) with the theory prediction (blue and red solid lines) and corresponding number histograms above (blue and red filling) at two different times (grey vertical lines). The solid lines are Gaussians obtained by fitting their sum to the histograms. All error bars denote the s.e.m.

interactions is dictated by the strong applied magnetic field, which causes isotropic interactions to emerge for the $\boldsymbol{B}_z$-configuration (Fig. 1b) used in the measurements of Fig. 2. Rotating the magnetic field permits tailoring of the anisotropy of the dressing-induced interactions, which is maximized by aligning the magnetic field with the wavevector $\boldsymbol{k}$ of the circularly polarized dressing laser in the plane of the spin lattice (Supplementary Fig. 4). The correlation measurements confirm the expected anisotropy, and we observe an aspect ratio of $\sim 3/2$, in quantitative agreement with the theory (Fig. 3b).

In addition to probing the coherent spin interactions, the applied interferometric technique allows an in-depth characterization and understanding of decoherence in the present system, which is of great importance for future applications of Rydberg dressing. The measured spin correlations (Fig. 2c) reveal an unexpected homogeneous offset, in addition to the characteristic spatial dependence. This requires a process affecting the system globally, and can be explained in terms of an additional dissipation channel triggering the loss of all particles in the dressed $|\uparrow\rangle$ state. Such a loss process is also consistent with the measured atom number distributions that steadily develop a bimodal structure with increasing dressing time (Fig. 4 and Supplementary Figs 5 and 6). Incoherent transitions to other Rydberg states due to black-body radiation present a plausible mechanism[24], since such transitions project the $|\uparrow\rangle$ state onto a nearby Rydberg state, and thereby produce a real Rydberg excitation (Supplementary Fig. 8). The production of such atoms with opposite parity with a small rate $\beta^2\gamma_{\mathrm{BB}}$ can induce strong dipolar exchange interactions, and thereby trigger a fast avalanche-like atom loss due to strong resonance broadening[24,38,39]. We can incorporate this picture into our theoretical description by assuming a stochastically triggered instantaneous loss of all $|\uparrow\rangle$-state atoms as a simplification, still permitting an analytical solution of the many-body dynamics (Supplementary Information). This loss process, being spatially uniform, does not modify the shape of the correlations, but leads to an overall scaling and can account for a uniform offset. Indeed, the measured correlations shown in Fig. 2 are well explained by this model and the offset is reproduced to within 20%. We extract a value of $\gamma_{\mathrm{BB}}/2\pi = 1.6\,\mathrm{kHz}$, approximately half the literature value for $31P_{1/2}$-states[36].

Furthermore, we observe a decreasing atom number N with increasing total dressing time t (Fig. 4), consistent with the predicted exponential loss $N(t) = N(0)\mathrm{e}^{-(N(0)/4)\beta^2\gamma_{\mathrm{bb}}t}$ (Supplementary Information). Due to the dependence on system size via $N(0)$, the extracted value of 130(20) μs is significantly lower than the anticipated value of $\tau_{\mathrm{r}}/\beta^2 = 2.2\,\mathrm{ms}$ in the absence of additional loss processes; however, it surpasses the bare Rydberg state lifetime by a factor of five. The spin-resolved measurement agrees equally well with the predicted dynamics, strongly supporting the developed understanding of the many-body dynamics.

The demonstrated spatio-temporal control over long-range spin interactions in a unity-filled lattice holds promise for a new generation of quantum simulation platforms. We anticipate that significant improvement in the current coherence time is possible in designed lattice systems with fewer spins or reduced dimensionality[18], an appropriately adjusted Rydberg-state detuning to avoid coupling to broadened resonances, or via stroboscopic dressing that allows detrimental impurity Rydberg atoms to decay or be laser-quenched[29] before triggering the avalanche loss. Our results pave the way towards experimental explorations of more complex quantum magnets[3,4,9] and the study of novel phenomena in Rydberg-dressed atomic lattices[26,27].

Data availability

The data that support the plots within this paper and other findings of this study are available from the corresponding author upon reasonable request.

Received 18 April 2016; accepted 21 June 2016;
published online 1 August 2016

References

1. Baranov, M. A., Dalmonte, M., Pupillo, G. & Zoller, P. Condensed matter theory of dipolar quantum gases. *Chem. Rev.* **112,** 5012–5061 (2012).
2. Balents, L. Spin liquids in frustrated magnets. *Nature* **464,** 199–208 (2010).
3. Glaetzle, A. W. *et al*. Designing frustrated quantum magnets with laser-dressed Rydberg atoms. *Phys. Rev. Lett.* **114,** 173002 (2015).
4. van Bijnen, R. & Pohl, T. Quantum magnetism and topological ordering via Rydberg dressing near Förster resonances. *Phys. Rev. Lett.* **114,** 243002 (2015).
5. Henkel, N., Nath, R. & Pohl, T. Three-dimensional roton excitations and supersolid formation in Rydberg-excited Bose–Einstein condensates. *Phys. Rev. Lett.* **104,** 195302 (2010).
6. Pupillo, G., Micheli, A., Boninsegni, M., Lesanovsky, I. & Zoller, P. Strongly correlated gases of Rydberg-dressed atoms: quantum and classical dynamics. *Phys. Rev. Lett.* **104,** 223002 (2010).
7. Santos, L., Shlyapnikov, G. V., Zoller, P. & Lewenstein, M. Bose–Einstein condensation in trapped dipolar gases. *Phys. Rev. Lett.* **85,** 1791–1794 (2000).
8. Bouchoule, I. & Mølmer, K. Spin squeezing of atoms by the dipole interaction in virtually excited Rydberg states. *Phys. Rev. A* **65,** 041803 (2002).
9. Glaetzle, A. *et al*. Quantum spin-ice and dimer models with Rydberg atoms. *Phys. Rev. X* **4,** 041037 (2014).
10. Trotzky, S. *et al*. Time-resolved observation and control of superexchange interactions with ultracold atoms in optical lattices. *Science* **319,** 295–299 (2008).
11. Lahaye, T., Menotti, C., Santos, L., Lewenstein, M. & Pfau, T. The physics of dipolar bosonic quantum gases. *Rep. Prog. Phys.* **72,** 126401 (2009).
12. Blatt, R. & Roos, C. F. Quantum simulations with trapped ions. *Nature Phys.* **8,** 277–284 (2012).
13. Saffman, M., Walker, T. G. & Mølmer, K. Quantum information with Rydberg atoms. *Rev. Mod. Phys.* **82,** 2313–2363 (2010).

14. Yan, B. *et al*. Observation of dipolar spin-exchange interactions with lattice-confined polar molecules. *Nature* **501,** 521–525 (2013).
15. Britton, J. W. *et al*. Engineered two-dimensional Ising interactions in a trapped-ion quantum simulator with hundreds of spins. *Nature* **484,** 489–492 (2012).
16. Richerme, P. *et al*. Non-local propagation of correlations in quantum systems with long-range interactions. *Nature* **511,** 198–201 (2014).
17. Jurcevic, P. *et al*. Quasiparticle engineering and entanglement propagation in a quantum many-body system. *Nature* **511,** 202–205 (2014).
18. Schauß, P. *et al*. Crystallization in Ising quantum magnets. *Science* **347,** 1455–1458 (2015).
19. Labuhn, H. *et al*. Tunable two-dimensional arrays of single Rydberg atoms for realizing quantum Ising models. *Nature* **534,** 667–670 (2016).
20. Weber, T. M. *et al*. Continuous coupling of ultracold atoms to an ionic plasma via Rydberg excitation. *Phys. Rev. A* **86,** 020702 (2012).
21. Balewski, J. B. *et al*. Rydberg dressing: understanding of collective many-body effects and implications for experiments. *New J. Phys.* **16,** 063012 (2014).
22. Malossi, N. *et al*. Full counting statistics and phase diagram of a dissipative Rydberg gas. *Phys. Rev. Lett.* **113,** 023006 (2014).
23. Schempp, H. *et al*. Full counting statistics of laser excited Rydberg aggregates in a one-dimensional geometry. *Phys. Rev. Lett.* **112,** 013002 (2014).
24. Goldschmidt, E. A. *et al*. Anomalous broadening in driven dissipative Rydberg systems. *Phys. Rev. Lett.* **116,** 113001 (2016).
25. Jau, Y.-Y., Hankin, A. M., Keating, T., Deutsch, I. H. & Biedermann, G. W. Entangling atomic spins with a Rydberg-dressed spin-flip blockade. *Nature Phys.* **12,** 71–74 (2016).
26. Mattioli, M., Dalmonte, M., Lechner, W. & Pupillo, G. Cluster Luttinger liquids of Rydberg-dressed atoms in optical lattices. *Phys. Rev. Lett.* **111,** 165302 (2013).
27. Li, X. & Sarma, S. D. Exotic topological density waves in cold atomic Rydberg-dressed fermions. *Nature Commun.* **6,** 7137 (2015).
28. Honer, J., Weimer, H., Pfau, T. & Büchler, H. P. Collective many-body interaction in Rydberg dressed atoms. *Phys. Rev. Lett.* **105,** 160404 (2010).
29. Schauß, P. *et al*. Observation of spatially ordered structures in a two-dimensional Rydberg gas. *Nature* **491,** 87–91 (2012).
30. Knap, M. *et al*. Probing real-space and time-resolved correlation functions with many-body Ramsey interferometry. *Phys. Rev. Lett.* **111,** 147205 (2013).
31. Carroll, T. J., Claringbould, K., Goodsell, A., Lim, M. J. & Noel, M. W. Angular dependence of the dipole–dipole interaction in a nearly one-dimensional sample of Rydberg atoms. *Phys. Rev. Lett.* **93,** 153001 (2004).
32. Barredo, D. *et al*. Demonstration of a strong Rydberg blockade in three-atom systems with anisotropic interactions. *Phys. Rev. Lett.* **112,** 183002 (2014).
33. Gil, L., Mukherjee, R., Bridge, E., Jones, M. & Pohl, T. Spin squeezing in a Rydberg lattice clock. *Phys. Rev. Lett.* **112,** 103601 (2014).
34. Schachenmayer, J., Lesanovsky, I., Micheli, A. & Daley, A. J. Dynamical crystal creation with polar molecules or Rydberg atoms in optical lattices. *New J. Phys.* **12,** 103044 (2010).
35. Mukherjee, R., Killian, T. C. & Hazzard, K. R. Accessing Rydberg-dressed interactions using many-body Ramsey dynamics. Preprint at http://arXiv.org/abs/1511.08856 (2015).
36. Beterov, I. I., Ryabtsev, I. I., Tretyakov, D. B. & Entin, V. M. Quasiclassical calculations of blackbody-radiation-induced depopulation rates and effective lifetimes of Rydberg nS, nP, and nD alkali-metal atoms with $n \leq 80$. *Phys. Rev. A* **79,** 052504 (2009).
37. Fukuhara, T. *et al*. Quantum dynamics of a mobile spin impurity. *Nature Phys.* **9,** 235–241 (2013).
38. Anderson, W. R., Veale, J. R. & Gallagher, T. F. Resonant dipole–dipole energy transfer in a nearly frozen Rydberg gas. *Phys. Rev. Lett.* **80,** 249–252 (1998).
39. Mourachko, I. *et al*. Many-body effects in a frozen Rydberg gas. *Phys. Rev. Lett.* **80,** 253–256 (1998).

Acknowledgements

We thank A. Glätzle, P. Zoller, M. Cheneau and N. Henkel for discussions. We acknowledge funding by MPG, EU (UQUAM, SIQS, RYSQ, HAIRS, Marie Curie Fellowship to J.-y.C.) and the Körber Foundation.

Author contributions

J.Z. performed the measurements; J.Z. and P.S. planned the experiment under the supervision of C.G. and I.B.; R.v.B. and T.P. developed the analytical model and the *ab initio* potential calculation. All authors contributed to interpreting the data and writing the manuscript.

Additional information

Supplementary information is available in the online version of the paper. Reprints and permissions information is available online at www.nature.com/reprints. Correspondence and requests for materials should be addressed to C.G.

Competing financial interests

The authors declare no competing financial interests.